Published in final edited form as:
J Mol Biol. 2014 October 23; 426(21): 3656–3669. doi:10.1016/j.jmb.2014.08.018.

A conserved isoleucine maintains the inactive state of Bruton's tyrosine kinase

Scott E. Boyken[1,#], **Nikita Chopra**[1,#], **Qian Xie**[1], **Raji E. Joseph**[1], **Thomas E. Wales**[2], **D. Bruce Fulton**[1], **John R. Engen**[2], **Robert L. Jernigan**[1], and **Amy H. Andreotti**[1,*]

[1]Roy J. Carver Department of Biochemistry, Biophysics and Molecular Biology, Iowa State University, Ames, IA 50011, USA

[2]Department of Chemistry and Chemical Biology, Northeastern University, Boston, MA 02115, USA

Abstract

Despite high homology among non-receptor tyrosine kinases, different kinase families employ a diverse array of regulatory mechanisms. For example, the catalytic kinase domains of the Tec family kinases are inactive without assembly of the adjacent regulatory domains, whereas the Src kinase domains are autoinhibited by the assembly of similar adjacent regulatory domains. Using molecular dynamic simulations, biochemical assays, and biophysical approaches, we have uncovered an isoleucine residue in the kinase domain of the Tec family member Btk that, when mutated to the closely related leucine, leads to a shift in the conformational equilibrium of the kinase domain toward the active state. The single amino acid mutation results in measureable catalytic activity for the Btk kinase domain in the absence of the regulatory domains. We suggest this isoleucine side chain in the Tec family kinases acts as a 'wedge' that restricts the conformational space available to key regions in the kinase domain, preventing activation until the kinase domain associates with its regulatory subunits and overcomes the energetic barrier to activation imposed by the isoleucine side chain.

Keywords

Tec kinase regulation; molecular dynamics; catalytic activity; active/inactive conformational equilibrium; isoleucine/leucine

Introduction

Protein kinases transfer the γ-phosphate of ATP to the side chain of a substrate molecule, serving as key mediators of cellular signaling pathways. Given the importance of this

*Corresponding author: amyand@iastate.edu.
#These authors contributed equally to this work

chemical modification in driving cellular responses to stimuli, kinase catalytic activity is tightly controlled. There are well-defined, conserved structural elements that must be appropriately assembled for catalysis, serving as hallmarks of an active kinase (Fig. 1a): the Lys/Glu salt bridge, the Regulatory spine (R-spine) (1–4), the αC helix, and the DFG motif (5). Phosphorylation of one or more hydroxyl-containing side chains in the activation loop (A-loop) triggers assembly of the active kinase conformation (Fig. 1a). Specifically, the activation loop phosphotyrosine attracts a conserved Arg in the same loop, pulling it away from an electrostatic interaction with a conserved Glu on the αC helix. This transition releases the αC-helix so that it switches from an 'αC-out' to 'αC-in' conformation, leading to the short distance (<4Å) between the side chains of the conserved Glu and a conserved Lys, forming a new electrostatic interaction characteristic of the active kinase (6). This electrostatic switch is accompanied by assembly of the Regulatory spine residues and a conformational shift in the DFG motif forming a hydrogen bond between the carboxylate side chain of the aspartate (Oδ1) and the backbone amide (NH) of the glycine.

Despite the fact that this set of structural features is present in all active kinases, it is clear that different kinases follow different regulatory rules. Striking examples are the Tec (7–10) and Src family tyrosine kinases (11, 12); these kinase families are closely related evolutionarily but employ opposing regulatory schemes. Tec kinase domains, even when phosphorylated on the activation loop, are inactive, relying on direct association with regulatory regions outside of the kinase domain to achieve activation (13–16). In contrast, phosphorylated Src family kinase domains are fully active by themselves (17, 18), and are inhibited by association with their regulatory domains (19, 20). This fundamental difference suggests that there are unique structural motifs within the Tec family that 'hold' these kinase domains in the inactive conformation until proper assembly with the adjacent regulatory domains.

Here we use a combination of computational methods, biochemical assays, and biophysical methods to identify the molecular determinants that are responsible for the 'inactive by default' status of the Tec family kinases. To identify the regulatory features within the Tec and Src family kinase domains that are responsible for the observed differences in catalytic efficiency, we focus on two specific kinases, Btk (one of five Tec family kinases) and Lck (one of nine Src family kinases); these specific kinases were chosen based on availability of high-resolution crystal structures of each kinase domain in the active conformation. Our findings point to an isoleucine residue conserved among the Tec family kinases, that acts as a 'wedge' restricting the conformational space available to key regulatory elements of the kinase domain. Removing the 'wedge' by mutation of isoleucine to leucine, the corresponding residue in the Src kinases, results in increased conformational sampling and leads to partial activation of the Tec family kinase domain in the absence of the otherwise necessary regulatory region. Elucidating the molecular details that account for the conformational preferences and respective activities of the Tec and Src family kinase domains is important for fully understanding the regulatory mechanisms that govern signaling through these kinases.

Results

Molecular Dynamics simulations reveal differences in the conformational preferences of Lck and Btk kinase domains

To explore the differences in the Lck and Btk kinase domains that differentially drive the assembly of the active catalytic core, we initialized all-atom Molecular Dynamics (MD) simulations starting from the active conformations of each kinase domain. PDB ID 3LCK was used as the starting structure for active Lck kinase domain and PDB ID 3K54 was used as the starting structure for active Btk kinase domain. We performed 100 ns equilibrium simulations in the Normal Pressure Temperature (NPT) ensemble, with three replicates for the Btk structure and two replicates for Lck. Throughout the simulations, RMSD was monitored from the starting structure for the hallmarks of the active catalytic core, as well as distances between specific residues involved in electrostatic interactions in and around the active site (Figs. 1b,c and S1a). The Lck kinase domain retains its active conformation throughout the entire 100 ns in both replicates (Fig 1b). This is consistent with a recent MD study showing that the Src kinase domain retains the active, assembled catalytic core during a simulation of 10 microseconds (21). In contrast, the Btk kinase domain deviates from its starting active structure early in the simulation (Fig. 1c). Structural changes in Btk are localized within the N-lobe of the kinase; the Btk αC helix moves away from the N-lobe, breaking the K430-E445 salt bridge and disassembling the Regulatory-spine (Fig. 1c). During the simulations, Btk samples inactive conformations observed in numerous Tec family kinase domain crystal structures in which the αC helix adopts the inactive 'αC-out' position but the A-loop is in the active "open" position. Additionally, the observed outward movement of the Btk αC helix led to formation of the R544/E445 salt bridge in one replicate, a structural feature that is observed in many inactive kinase domain structures (Fig. S1b).

Given the differences in the simulations of Btk and Lck, we set out to identify molecular features that lead to the spontaneous conformational shift away from the active Btk kinase domain structure. We focused on the αC helix since the most pronounced changes occur in this region of the structure during the course of the simulation. Assessing the relative structural stability conferred by local interactions within protein kinases has proven useful in determining the molecular basis of cancer causing mutations that likely alter the conformational preferences of a kinase domain (22). The hypothesis is that specific side chains that cannot form optimal contacts within the surrounding structure will be a driving force for conformational changes that allow for optimal interactions. Drawing an analogy to that work, we performed mutational frustration analysis (see Methods) (23–25) at 0, 10, and 100 ns time points from the Btk simulation. A number of frustrated contacts are evident for residues on the αC helix early in the simulation and these non-optimal contacts are resolved as the αC helix moves to the 'αC-out' conformation (Fig. S2a). Four αC helix residues, E439, E441, F442 and E445, participate in the majority of the frustrated contacts at early time points in the simulations (Fig. S2b), indicating that these sites are likely regions of local instability in the structure of the active Btk kinase domain. Since these frustrated αC helix residues all face the N-lobe, we reasoned that mutation of these amino acids might relieve the non-optimal contacts and stabilize the active, 'αC-in' conformation of the Btk kinase

domain. E439 and E441 are unique to the Tec family kinases (not conserved in Src kinases) and so these Btk residues are targets for mutagenesis to the corresponding residues in Lck (E439P, E441A).

The other two residues on the αC helix identified by frustration analysis, F442 and E445, are completely conserved throughout the Tec and Src family kinases and so direct mutation of these residues was not pursued. However, the fact that these residues are at the hub of a locally frustrated region within the active Btk kinase domain structure prompted us to examine amino acids interacting with F442 and E445, using a contact radius of 6Å (Fig. S2c). Excluding residues on the αC helix itself, we find that F442 and E445 are within 6 Å of the side chains of eight different residues in the Btk kinase domain: K430, I432, V463, T465, I470, I472, D539, and F540 (Fig. S2c). Seven of these amino acids (underlined in the list above) are either conserved across both the Tec and Src family kinases or are present in certain members of both families. Btk I432 is unique as it is conserved among the Tec kinases but not present in any of the Src family kinases. In the Src kinases this residue corresponds to either leucine or methionine. Thus, in addition to the Btk E439P and E441A mutations, mutation of Btk I432 to a leucine (present in Lck) is also a candidate for further characterization by *in vitro* kinase assays.

Mutation of isoleucine 432 to leucine relieves the inactive by default status of the Btk kinase domain

Based on analysis of the MD simulations, three mutations (I432L, E439P, and E441A) were introduced together and separately into the His-tagged Btk kinase domain and each protein was expressed and purified. Btk kinase activity was first assessed by western blot to measure autophosphorylation using a phosphotyrosine specific antibody for the phosphorylation site (Y551) on the Btk activation loop (Fig. 2a). Activation loop phosphorylation is commonly used as a qualitative indicator of kinase activity (26, 27). Western blot analysis indicates that the triple mutant (Btk IEE/LPA) is more active than wild type Btk, consistent with analysis of the Btk simulation data suggesting that I432, E439 and E441 contribute to the destabilization of the active Btk conformation. For the separate mutations, I432L activates Btk whereas the E439P and E441A do not (Fig. 2a). Initial velocity measurements for phosphorylation of the poly (4:1 Glu, Tyr) peptide also show that Btk I432L is catalytically more active than wild type Btk for this generic substrate (Fig. 2b). The 5-fold activity increase (V_i/[Enzyme] = ~0.5 for Btk I432L and V_i/[Enzyme] = ~0.1 for isolated Btk kinase domain) can be compared with that of full length Btk to assess the extent of activation realized by the I432L mutation. The previously published initial velocity data for full length Btk, V_i/[Enzyme] = 2 min^{-1} (14), suggests that the I432L mutation in the Btk kinase domain activates the isolated Btk kinase domain to 25% of that of the full-length enzyme. It should be noted here that the previously characterized full length Btk protein was expressed and purified from insect cells rather than the bacterial expression system used here for the kinase domain fragments.

To further characterize the I432L mutation we made use of a previously published mutant Btk kinase domain, Btk Y617P (28). The Y617P mutation is located in the C-lobe of the kinase domain and results in higher yield from bacteria than the wild type Btk kinase

domain, facilitating more detailed enzymology and biophysical characterization. We have previously noted that the Y617P mutation enhances the basal activity of the Btk kinase domain by an unknown mechanism and so we first wished to assess whether the I432L mutation causes the same activation in this background compared to wild type Btk kinase domain. Using autophosphorylation of Y551 as a qualitative indicator of activity, we find that the Btk Y617P/I432L kinase domain retains the activity enhancement over the Btk Y617P kinase domain observed for the wild type kinase domain and I432L single mutant (Fig. 2c). We therefore proceeded with quantitative assays to determine K_M and k_{cat} values for the Btk Y617P kinase domain with and without the I432L mutation. Peptide substrate curves were generated using Peptide B (aminohexanoyl biotin-EQEDEPEGIYGVLF-NH_2) and the data were fit to determine K_M and k_{cat} values for the Btk kinase domain and the I432L mutant kinase domain (Fig. 2d). The Btk Y617P/I432L mutant kinase domain exhibits a k_{cat} value = 12.2±1.3 min^{-1}, seven times faster than k_{cat} = 1.7±0.2 min^{-1} for the Btk kinase domain carrying the wildtype isoleucine at position 432. The K_M value for the Btk I432L mutant kinase domain does not change significantly from that of the Btk kinase domain (K_M(Btk Y617P) = 179 ± 40 μM; K_M(Btk Y617P/I432L) = 275 ± 57 μM). To ensure the observed activity differences are not arising due to stability differences between Btk Y617P and Btk Y617P/I432L, we measured thermal denaturation curves for both proteins and find that the more active Btk Y617P/I432L kinase domain is in fact slightly less stable than Btk Y617P kinase domain (Fig. S3). The Btk kinase domain Y617P/I432L mutant exhibits a T_m = 43 °C compared to T_m = 44.5 °C for the Btk kinase domain Y617P. Thus, results of qualitative western blot analysis, initial velocity measurements, and peptide phosphorylation kinetics all show that substitution of the isoleucine at position 432 with leucine increases the catalytic activity of the isolated Btk kinase domain.

We next carried out 50 ns simulations for Btk I432L, using the same starting conformation (3K54) and parameters as the simulations in Figure 1 (Figs. 3a, S2d). Throughout the simulation, the Btk I432L mutant retains the hallmarks of an active kinase (Fig. 3a) to a greater extent than the corresponding simulation of the wild type Btk kinase domain (Fig. 1c). At the end of the simulation, the leucine side chain introduced at position 432 in Btk has rotated around the Cα-Cβ bond to adopt the trans chi1 rotamer conformation creating space for the F442 side chain on the C-helix (Fig. 3b). The resulting ‘αC-in’ conformation appears stabilized by favorable contacts between the F442 side chain and the side chains of L432 and I472; the latter residue is conserved in both Tec and Src kinases. The final structure surrounding F442 in the simulation of the Btk I432L kinase domain is very similar to the structure of the Lck kinase domain throughout its entire simulation (Fig. 3c).

This analysis of the Btk I432L mutant prompted closer inspection of the I432 rotamer population in the wild type Btk crystal structure and simulation data. The precise position of the isoleucine side chain atoms in the Btk kinase domain structure is uncertain due to poor side chain electron density. The reported B-factors for this region of the structures are high, consistent with flexibility or uncertainty in this region. We therefore used the simulation data to monitor rotamer occupancies over time for the I432 side chain. Plotting the Btk I432 chi1 angle as a function of simulation time reveals multiple rotameric states with a preference for the gauche(+) and gauche(−) rotamers (chi1 = ±60°) and only a transient

occupancy of the trans rotamer (chi1 = ±180°) (Fig. 4a–c). The I432 gauche(+) chi1 angle results in the delta methyl group (Cδ) of I432 pointing directly toward F442 on the αC helix providing a steric block to the 'αC-in' conformation that is required for the active kinase (Fig. 4b). The gauche(−) chi1 angle for I432 also places the sterically bulky isoleucine side chain in a position that blocks F442 (Fig. 4c).

The same chi1 analysis for the corresponding leucine for both Lck (L275) and the Btk I432L mutant, suggests that in these cases the non-beta branched leucine side chain predominantly occupies the trans rotamer (Fig. 4d,e) as already observed at the end point of the Btk I432L simulation (Fig. 3b). The trans leucine rotamer does not sterically block the phenylalanine side chain on the αC helix resulting in an increase in the conformational space available to the αC helix of Lck and Btk I432L (Fig. 4f). Moreover, L275 in the Lck kinase domain structure has low B-factors for the side chain atoms indicating that the trans chi1 angle is a stable conformation in the crystal.

The simulation data suggest that the steric effect of the I432 side chain on the local structure of the Btk kinase domain N-lobe, in particular the phenylalanine on the αC-helix, is distinct from that of the corresponding leucine in the Src family kinases. The rotameric preferences of the beta-branched I432 side chain seem to create a wedge that limits the conformational space available to the Btk αC helix in the isolated Btk kinase domain (Fig. 5a, *left*). Mutation of Btk I432 to the non-beta-branched leucine opens the hydrophobic surface formed by L432 and I472 (see Fig. 3b) to accommodate the side chain of F442. In a similar manner, we suggest that the conformational preference of the native isoleucine side chain in wild type Btk could shift to the trans chi 1 rotamer upon activation by the associated regulatory domains of Btk, creating space for F442 and allowing the αC helix to more readily sample the 'αC-in' conformation of the active kinase domain (Fig. 5a, *right*).

The proposed model predicts that, in full length Btk, the non-catalytic regulatory region provides sufficient stabilization energy to overcome the intrinsic conformational preference of the isolated kinase domain for the inactive state, presumably shifting the I432 chi1 rotamer population toward the trans conformation resulting in greater sampling of the active conformation. To test this hypothesis, we introduced the I432L mutation into full length Btk and compared the activity of this mutant with the non-mutated full length Btk kinase. The activity of full length Btk and full length Btk I432L are indistinguishable by western blot analysis probing activation loop (pY551) phosphorylation levels (Fig. 5b). In this experiment we probed activation loop phosphorylation levels before and after incubation with ATP to show that both proteins, when purified, start at the same (low) level of phosphorylation on Y551. The corresponding experiment for the isolated Btk kinase domain demonstrates the activating effect of I432L (Fig. 5c) after incubation with ATP as already shown in Figure 2.

The I432L mutation alters the conformational equilibrium of the Btk kinase domain

To experimentally test the hypothesis that the Btk I432L mutant is more active than wild type Btk kinase domain due to differences in the conformational space available to the αC helix, we turned to NMR spectroscopy to measure the dynamics of residues in this region of the Btk kinase domain. The resonance frequency of every hydrogen (^{1}H) that is directly

attached to a nitrogen (^{15}N) is measured using a TROSY (transverse relaxation–optimized spectroscopy) version of the heteronuclear single quantum correlation (HSQC) spectrum (29). The resulting data provides a direct measure of the chemical environment and dynamical properties of each amide NH group in the protein. Comparison of the ^{1}H-^{15}N TROSY HSQC spectrum of uniformly ^{15}N labeled Btk kinase domain with that of ^{15}N labeled Btk I432L reveals linewidth differences for a subset of peaks indicative of dynamic differences in specific regions of the two proteins (Fig. 6a,b). Overall, NMR linewidths are broader for the Btk I432L mutant than wild type Btk suggesting that the activated mutant is more dynamic. Complete backbone resonance assignments for the Btk kinase domain are not available and so we have pursued selective isotopic labeling to obtain chemical shift assignments for the phenylalanine backbone amide resonances in the Btk kinase domain (27, 28).

In the present work, the amide resonance corresponding to F442 on the αC helix could not be unequivocally assigned. Having previously assigned the backbone amide of F540 (27), we examined its resonance in ^{1}H-^{15}N TROSY HSQC spectra of the Btk wild type and I432L mutant kinase domains. The location of F540 within the conserved DFG motif places it close in space to the αC helix (Figs. 1a) where it is likely to report on dynamic changes that result from substitution of I432 with leucine. Indeed, a peak corresponding to F540 is present in the ^{1}H-^{15}N TROSY HSQC of wild type Btk, but is absent in the spectrum of Btk I432L, due to line broadening and/or a significant resonance frequency change, (Fig. 6a,b). The absence of new peaks in the spectrum of Btk I432L kinase domain that are not present in the wild type data favors line broadening to explain the disappearance of the F540 amide resonance. The significant change in the F540 resonance combined with observation of overall line broadening in the spectrum of Btk I432L, is consistent with an increase in conformational exchange on the μsec or faster timescale (30) in the more active Btk I432L mutant.

The spectral changes in the F540 amide resonance that are observed upon mutation of I432 to leucine prompted us to compare the DFG motif in simulations of wild type Btk with that of the Btk I432L mutant. The DFG motif in all available crystal structures of the Btk kinase domain adopts a conformation that is not optimal for an active kinase. More specifically, the Btk 3K54 crystal structure has a DFG motif that is similar to the ‘DFG-in’ conformation, but the carboxylate side chain of D539 (Oδ1) does not form a hydrogen bond to the backbone amide (NH) of G541 (Fig 6c, *left*). Moreover, in simulations of wild type Btk kinase domain, the distance between Oδ1 of D539 and the backbone amide nitrogen (N) of G541 varies between 6 and 8 Å suggesting that the hydrogen bond is never significantly populated (Fig. 6c, *right*). In contrast, during the simulation of the Btk I432L mutant, the DFG motif adopts a conformation in which the aspartate Oδ1 is <3.5 Å from the glycine backbone amide (N), consistent with formation of a hydrogen bond (Fig. 6d, *right*). In one of the two replicates the hydrogen bond is maintained for a significant time during the simulation while the short distance between Oδ1 and N is only transiently populated in the other replicate. A snapshot of the Btk I432L kinase domain during the simulation shows formation of the Oδ1/NH hydrogen bond within the DFG motif (Fig. 6d, *left*). The DFG conformation observed in the Btk I432L simulation is indistinguishable from that in the active structure of

Lck. Thus, NMR data combined with MD simulations suggest that mutation of I432 to leucine within Btk results in conformational sampling of the optimal 'DFG-in' structure associated with the active state of protein kinases.

To further probe the dynamic characteristics of the Btk I432L mutant we compared the solution behavior of Btk kinase domain with the Btk I432L kinase domain mutant by hydrogen-deuterium exchange mass spectrometry (HDXMS). HDXMS allows detection of backbone amide hydrogens for each amino acid in the protein (except proline) so that a direct comparison of the solvent accessibility/H-bonding of the amide N-H can be made for wild type Btk and the Btk I432L mutant. Comparison of the hydrogen exchange behavior for Btk I432L versus wild type Btk showed measurable changes in deuterium incorporation in the kinase domain for the I432L mutant (Fig. 7a, Fig. S4). Most of the changes in deuterium exchange are localized in the N-lobe of the kinase, with the C-lobe remaining relatively unperturbed. The largest differences in deuterium uptake are observed in peptides that cover the β2 strand, the β2-β3 loop, and the N-terminal end of the activation loop in the Btk I432L mutant compared to wild-type Btk (Fig. 7a,b). For these regions of secondary structure, the Btk I432L mutant exchanges more readily than wild type Btk suggesting the mutant protein samples more open conformations than wild type Btk. The Btk I432L mutant also shows small differences in deuterium uptake for part of the β3 strand, β4 strand, β4-β5 loop, β5 strand, β6 strand, β6-β7 loop, β7 strand (including the DFG motif), the catalytic loop and the C-terminal end of the activation segment (Fig. 7b,c,d). In these peptide regions as well, Btk I432L showed increased deuterium incorporation, although more moderate, when compared to wild type Btk. It is also interesting to note that hydrogen/deuterium exchange does not differ between the two proteins for the αC helix itself suggesting that amide hydrogen accessibility within this region of secondary structure is not affected by the mutation. Thus, to the extent that the αC helix samples greater conformational space in the Btk I432L mutant, it does so in a concerted fashion without changes to the helical structure.

Discussion

Leucine and isoleucine are structural isomers that are often considered interchangeable due to their related hydrophobic side chains (31, 32). At the same time, it is appreciated that the beta-branched isoleucine side chain introduces conformational restrictions that can either stabilize or destabilize the polypeptide chain depending upon context (33). For Btk and the Tec family kinases, MD simulation data suggest that specific chi 1 rotamers of the isoleucine at position 432 in the kinase domain sterically maintains the inactive kinase domain conformation (αC helix out) in the absence of the Btk regulatory domains. Mutation of the I432 to the non-beta branched leucine likely shifts the rotamer preference at this position leading to changes in protein motions and an increase in activity for the isolated Btk kinase domain. Indeed, the I432L mutation selectively affects k_{cat} and not K_M consistent with the notion that this mutation allows the Btk kinase domain to more frequently sample the active state.

In the full length Btk kinase, assembly of the non-catalytic regulatory domains onto the Btk kinase domain shift the conformational preference of the kinase domain to the active state, superseding the effects of the leucine substitution that are evident in the isolated kinase

domain. Presumably, in the controlled signaling pathways of Btk, negative regulatory signals would promote release of the Btk kinase domain from interactions with the regulatory domains, leading to a conformational shift in the kinase domain toward the inactive state. The shift from active to inactive state is driven in part by the conformational preferences of the I432 side chain within the released Btk kinase domain.

Mutations that favor the 'αC-in' conformation of any kinase could result in hyperactivation. Mutation of F457 (corresponds to F442 in Btk) to leucine in the Tec family kinase Bmx is reported in the Catalogue of Somatic Mutations in Cancer (COSMIC) database (34, 35). The phenylalanine to leucine mutation changes the face of the αC helix in Bmx and the less sterically demanding leucine side chain may pack more favorably with the isoleucine in Bmx (I447) leading to increased catalytic activity of the Bmx F457L kinase domain. Along these lines, it is also interesting to note that a leucine to phenylalanine mutation at the position corresponding to Btk I432 within the B-Raf kinase (L485F) is reported in the COSMIC database. Given the conserved phenylalanine on the αC helix (B-Raf F498 corresponding to F442 in Btk) it is tempting to speculate that a phenylalanine in place of leucine on the β3 strand of B-Raf might form favorable pi stacking interactions with F498 on the αC helix stabilizing the active 'αC-in' conformation. These reports collectively suggest that side chain packing in the region defined in this study can have significant effects on kinase catalytic activity. These effects may not be limited to kinases, as activity changes due to mutation of isoleucine to leucine have been characterized for several non-kinase systems (36–38). In one example, the human prolactin receptor is activated by mutation of an isoleucine to leucine resulting in dynamical changes and stabilization of the active state (39).

Both NMR spectroscopy and HDXMS support a model in which the Btk kinase domain experiences greater dynamic flexibility in the active state compared to the inactive state. The increase in deuterium incorporation suggests that the Btk I432L protein samples more open conformations than the wild type Btk kinase domain. NMR analysis of the phenylalanine in the DFG motif of Btk (F540) reveals differences in the relaxation properties of this residue in the context of Btk wild type versus Btk I432L. Given the proximity of the DFG motif to the αC helix, the observed increase in exchange broadening for the backbone amide of F540 in Btk I432L may reflect the nearby αC helix sampling greater conformational space that includes the 'αC-in' conformation associated with the kinase active state. In view of the well-characterized conformational shift of the DFG motif between active and inactive kinase structures (3), it is tempting to speculate that the slower conformational fluctuations on the microsecond timescale within Btk I432L evident in the NMR data may reflect exchange between DFG conformations. Along these lines, it is interesting to note that the optimal 'DFG-in' state is not observed in the crystal structures of Btk, perhaps another consequence of destabilization of the active state by I432. Indeed, the importance of the interplay between the DFG motif, the regulatory spine (which includes the DFG phenylalanine) and the stability of the active kinase has been recently addressed in related work on PKA (40) and together these findings emphasize the importance of the DFG phenylalanine in the assembled regulatory spine. Finally, the microsecond time scale motions detected for the DFG motif in the more active form of Btk (I432L) may also contribute directly to catalysis as has been suggested for other systems (41–43).

The increasing power of molecular dynamics simulations coupled with experiment offers a promising approach to elucidate the molecular determinants that control enzyme activity and regulation (21, 44). Our combined use of computation and experiment suggests that a single, conserved isoleucine residue is at least partly responsible for keeping Tec family kinase domains inactive until upstream signaling events trigger association between the non-catalytic regulatory region and kinase domain (14). Future work will aim to elucidate yet unidentified sequence and/or structural features that cooperate with the isoleucine 432 to drive the conformational equilibrium of the Tec family kinase domains toward the inactive state in the absence of the non-catalytic regulatory domains. A full mechanistic understanding of how the conformational equilibrium of the Tec kinase domains is controlled may lead to new opportunities in kinase inhibitor development. Additionally, the structural features exploited by the Btk kinase domain to favor the inactive conformation could provide clues and/or inspiration in drug discovery efforts aimed at inhibiting kinase domains that, unlike Btk, are active by default.

Materials and Methods

Structure preparation for simulations

Initial coordinates were obtained from the Protein Data Bank (PDB): 3K54 for active Btk kinase domain, and 3LCK for active Lck kinase domain. The starting structures consisted of the single kinase domains in the apo state (absent ATP or inhibitor), corresponding to aa 396–659 for Btk, and aa 239–501 for Lck. Both 3K54 and 3LCK contain a linker region N-terminal to the kinase domain that has been removed in order to monitor the effects of the isolated kinase domains and ensure identical domain boundaries for direct comparison of Btk to Lck. Regions missing from the electron density maps were modeled using MODELLER (45) and related active kinase domain structures as templates (see details in Supplemental Data). In all of the simulation systems, the kinase domains were phosphorylated, using the phosphotyrosine patch TP2, at the Tyr residue of the activation loop (Y551-Btk, Y394-Lck) to reflect the physiological state of the active kinase. The 3LCK crystal structure is phosphorylated at this position and the 3K54 crystal structure contains the Y551E phosphomimetic mutation at this position that was changed in silico to pY551. The I432L mutant structure was generated using MODELLER (45) and SCWRL 4(46).

Simulation setup

All-atom Molecular Dynamics simulations were performed using the CHARMM27(47) force field and TIP3P explicit water model in the NAMD 2.8 program (48). The simulation systems were solvated in a periodic water box with 15 Å buffering distance between protein surface and the box. Na^+ and Cl^- ions were added to neutralize the charge of the system, with a final molar concentration of approximately 150mM. Systems were equilibrated and simulated in the NPT ensemble at 310 K and 1 atm, using Particle-Mesh Ewald for long-range electrostatics. The cutoff used for the van der Waals and short-range electrostatics calculations was 12 Å and covalent hydrogens were kept rigid using the ShakeH algorithm. The simulation systems consisted of ~51000 atoms. The time step used was 2 fs. Simulation systems were first minimized (20 picoseconds (ps)) and equilibrated (50 ps) holding the protein rigid, allowing water molecules and Na^+ and Cl^- ions to move. The modeled loops

were then subjected to a short minimization to remove steric clashes. Next, the entire system was minimized, gradually releasing harmonic constraints on all protein heavy-atoms. The temperature of the system was then raised from 200 K to 310 K (5 K increments over 90 ps) with harmonic constraints on all protein heavy-atoms. Subsequently, the harmonic constraints were gradually released and the system was equilibrated for a total time of approximately 1 ns before starting production runs for analysis.

Analysis of simulation trajectories

Analysis of MD trajectories was carried out using VMD (49) and MATLAB (The Mathworks, Inc.). For RMSD calculations, superposition was based on the backbone atoms of the C-lobe, which in all simulations showed minimal movement, using the minimized starting structure for that simulation as the reference. Salt bridge distances were measured in VMD using the distance between the center of mass of the oxygens in the negatively charged side chain and the center of mass of the nitrogen in the positively charged side chain. Snapshots at 10 ns intervals were submitted to the Frustratometer server (50) (25). Mutational frustration scores, both pairwise and single-residue, were extracted from this analysis and used to identify frustrated residues. A Frustration Index (or z-score) ≥ 0.78 is minimally frustrated and < -1.0 is highly frustrated. Figures were generated using PyMOL (51).

Protein Expression, Purification and in vitro kinase assays

Btk mutants were generated by site-directed mutagenesis (Quikchange II kit, Stratagene). All constructs were confirmed by sequencing at the Iowa State University DNA synthesis and sequencing facility. His6-tagged Btk (residues 369–659) kinase domains (wild type and mutants used for Fig. 2a & b) are expressed in Arctic Express BL21(DE3) cells (Stratagene). Btk constructs (both kinase domain fragment and full length) containing the previously described Y617P mutation (28) are expressed in BL21(DE3) cells. Proteins used for enzymatic analysis and NMR spectroscopy are purified as previously described (52). Full length Btk Y617P and Btk Y617P/I432L are co-expressed with YopH to improve expression yield. Proteins used for HDXMS were further purified on a Hiload 75 (GE Healthcare) gel filtration column, concentrated to 80 μM, snap frozen in 100 μL aliquots and stored at −80 °C.

Kinase assays were performed as in Joseph *et al.* (15) using either wild type Btk kinase domain and the corresponding Btk mutants (I432L, E439P, E441A, and IEE/LPA) or Btk kinase domain Y617P and the corresponding Btk Y617/I432L mutant as indicated. Kinase reactions were carried out using 300 nM enzyme and analyzed by western blot and activity detected with anti-Btk pY551 antibody (BD Biosciences). Kinase assays involving the poly (4:1 Glu, Tyr) peptide substrate were carried out at room temperature by incubating the enzyme in a reaction buffer of 50 mM Hepes (pH 7.0), 10 mM $MgCl_2$, 1 mM dithiothreitol (DTT), 1 mg/mL bovine serum albumin (BSA), 1 mM Pefabloc, 5 mCi ^{32}P-ATP, 5 mg/ml poly (4:1 Glu, Tyr) peptide (Sigma) and 200 μM ATP. The peptide substrate was captured on a P-81 membrane (Whatman), washed thrice with 0.1% Phosphoric acid, once with 70% ethanol, dried and counted by scintillation counting. Full-length Btk enzymes and Btk kinase domains used in the kinase assays shown in Figure 5 are co-expressed with YopH to

eliminate activation loop phosphorylation prior to initiating the kinase assay (53). As a result, kinase assays using proteins produced in this way include the phosphatase inhibitor, sodium orthovanadate (1 mM). Kinetic parameters for Btk kinase domain Y617P and Btk kinase domain Y617P/I432L are derived using radioactive assays as follows: 1 μM Btk kinase domain Y617P or Y617PI432L mutant was incubated with peptide B substrate (aminohexanoyl biotin-EQEDEPEGIYGVLF-NH_2, a previously identified Tec family kinase substrate (16)). Peptide concentrations ranged from 0–550 μM in the reaction buffer (50 mM HEPES pH 7.0, 10 mM $MgCl_2$, 1 mM DTT, 1 mg/ml bovine serum albumin, 1 mM Pefabloc, 200 μM ATP and 5 μCi of [^{32}P]ATP (Perkin Elmer)) at room temperature. At 10-min and 20-min reaction times, 10 μl of the reaction mixture was removed and mixed with 5 μl of 8M guanidine hydrochloride to terminate the reaction. 10 μl of this reaction mixture was then spotted onto the biotin capture membrane (Promega), washed and the radioactivity incorporated on the peptide B substrate was quantified by scintillation counting. Each assay was performed in duplicate. The initial velocity of phosphorylation was then derived and K_M and k_{cat} values were obtained from fitting the data to the Michaelis Menten equation using GraFit.

NMR spectroscopy

Uniformly ^{15}N-labeled isolated kinase domains of Btk wild type or Btk I432L (both containing the Y617P mutation) were produced in *E. coli* BL21(DE3) cells, as described previously (28). ^{15}N-Phenylalanine labeled samples were produced by growing the *E. coli* BL21(DE3) cells in modified minimal media as described (28). The purified proteins were concentrated and dialyzed into buffer consisting of 50 mM Bicine (pH 8.0), 75 mM NaCl, 2 mM DTT, 5% glycerol and 0.02% NaN_3. All NMR spectra were collected at 298 K on a Bruker AVII 700 spectrometer equipped with a 5-mm HCN z-gradient cryoprobe operating at a ^{1}H frequency of 700.13 MHz. All data were analyzed with NMRViewJ software (54).

Hydrogen/deuterium exchange mass spectrometry (HDXMS)

Btk kinase domain samples for HDXMS contain a Y551F mutation on the kinase activation loop to prevent complications in the analysis due to differential phosphorylation. Deuterium labeling was initiated with an 18-fold dilution of an aliquot (80 pmoles) of Btk wild type and Btk I432L (both containing Y617P) into a buffer containing 99.9 % D_2O, 20 mM Tris, 150mM NaCl, 10% glycerol, pD 8.01. The labeling reaction was quenched with the addition of an equal volume of quench buffer [150 mM potassium phosphate (pH 2.47)]. Quenched samples were immediately frozen on dry ice until required for liquid chromatography-mass spectrometry (LC-MS) analysis. Quenched samples were rapidly thawed and injected into a Waters nanoACQUITY with HDX technology (55) for online pepsin digestion and ultra performance liquid chromatography (UPLC) separation of the resulting peptic peptides, and analyzed as reported previously (56). All mass spectra were acquired with a WATERS SYNAPT G2 HDMS mass spectrometer. The data were analyzed with DynamX 2.0 software. Relative deuterium amounts for each peptide were calculated by subtracting the average mass of the undeuterated control sample from that of the deuterium-labeled sample for isotopic distributions corresponding to the +1, +2, or +3 charge state of each peptide. The data were not corrected for back exchange and are therefore reported as relative values (57, 58). Differences larger than 0.4 Da are considered subtle while those larger than 0.8 Da

are considered obvious, according to the statistical criteria for relative HDXMS measurements previously described (59).

Supplementary Material

Refer to Web version on PubMed Central for supplementary material.

Acknowledgments

We thank Dr. Michael Zimmermann for beneficial discussions. Computing resources used to carry out the molecular dynamics simulations were obtained through a research allocation from the National Science Foundation's (NSF) Extreme Science and Engineering Discovery Environment (XSEDE) initiative. The YopH construct used for kinase expression was kindly provided by John Kuriyan. This work is supported by grants from the National Institutes of Health: AI043957 to A.H.A., GM101135 to J.R.E. and GM072014 to R.L.J.

References

1. Kornev AP, Haste NM, Taylor SS, Eyck LF. Surface comparison of active and inactive protein kinases identifies a conserved activation mechanism. Proc Natl Acad Sci U S A. 2006; 103:17783–17788. [PubMed: 17095602]
2. Kornev AP, Taylor SS, Ten Eyck LF. A helix scaffold for the assembly of active protein kinases. Proc Natl Acad Sci U S A. 2008; 105:14377–14382. [PubMed: 18787129]
3. Taylor SS, Kornev AP. Protein kinases: evolution of dynamic regulatory proteins. Trends Biochem Sci. 2011; 36:65–77. [PubMed: 20971646]
4. Kornev AP, Taylor SS. Defining the conserved internal architecture of a protein kinase. Biochim Biophys Acta. 2010; 1804:440–444. [PubMed: 19879387]
5. Nolen B, Taylor S, Ghosh G. Regulation of protein kinases; controlling activity through activation segment conformation. Mol Cell. 2004; 15:661–675. [PubMed: 15350212]
6. Kumar S, Nussinov R. Close-range electrostatic interactions in proteins. Chembiochem. 2002; 3:604–617. [PubMed: 12324994]
7. Andreotti AH, Schwartzberg PL, Joseph RE, Berg LJ. T-cell signaling regulated by the Tec family kinase, Itk. Cold Spring Harb Perspect Biol. 2010; 2(7):a002287. [PubMed: 20519342]
8. Joseph RE, Andreotti AH. Conformational snapshots of Tec kinases during signaling. Immunol Rev. 2009; 228:74–92. [PubMed: 19290922]
9. Schwartzberg PL, Finkelstein LD, Readinger JA. TEC-family kinases: regulators of T-helper-cell differentiation. Nat Rev Immunol. 2005; 5:284–295. [PubMed: 15803148]
10. Berg LJ, Finkelstein LD, Lucas JA, Schwartzberg PL. Tec family kinases in T lymphocyte development and function. Annu Rev Immunol. 2005; 23:549–600. [PubMed: 15771581]
11. Au-Yeung BB, et al. The structure, regulation, and function of ZAP-70. Immunol Rev. 2009; 228:41–57. [PubMed: 19290920]
12. Xu W, Doshi A, Lei M, Eck MJ, Harrison SC. Crystal structures of c-Src reveal features of its autoinhibitory mechanism. Mol Cell. 1999; 3:629–638. [PubMed: 10360179]
13. Joseph RE, Andreotti AH. Controlling the activity of the Tec kinase Itk by mutation of the phenylalanine gatekeeper residue. Biochemistry. 2011; 50:221–229. [PubMed: 21138328]
14. Joseph RE, Min L, Andreotti AH. The Linker between SH2 and Kinase Domains Positively Regulates Catalysis of the Tec Family Kinases. Biochemistry. 2007; 46:5455–5462. [PubMed: 17425330]
15. Joseph RE, Xie Q, Andreotti AH. Identification of an allosteric signaling network within Tec family kinases. J Mol Biol. 2010; 403:231–242. [PubMed: 20826165]
16. Hawkins J, Marcy A. Characterization of Itk tyrosine kinase: contribution of noncatalytic domains to enzymatic activity. Protein Expr Purif. 2001; 22:211–219. [PubMed: 11437596]
17. Yamaguchi H, Hendrickson WA. Structural basis for activation of human lymphocyte kinase Lck upon tyrosine phosphorylation. Nature. 1996; 384:484–489. [PubMed: 8945479]

18. Weijland A, et al. The purification and characterization of the catalytic domain of Src expressed in Schizosaccharomyces pombe. Comparison of unphosphorylated and tyrosine phosphorylated species. Eur J Biochem. 1996; 240:756–764. [PubMed: 8856081]
19. Gonfloni S, et al. The role of the linker between the SH2 domain and catalytic domain in the regulation and function of Src. EMBO J. 1997; 16:7261–7271. [PubMed: 9405355]
20. LaFevre-Bernt M, et al. Intramolecular regulatory interactions in the Src family kinase Hck probed by mutagenesis of a conserved tryptophan residue. J Biol Chem. 1998; 273:32129–32134. [PubMed: 9822689]
21. Shan Y, et al. Oncogenic mutations counteract intrinsic disorder in the EGFR kinase and promote receptor dimerization. Cell. 2012; 149:860–870. [PubMed: 22579287]
22. Dixit A, Verkhivker GM. The energy landscape analysis of cancer mutations in protein kinases. PLoS One. 2011; 6:e26071. [PubMed: 21998754]
23. Ferreiro DU, Hegler JA, Komives EA, Wolynes PG. On the role of frustration in the energy landscapes of allosteric proteins. Proc Natl Acad Sci U S A. 2011; 108:3499–3503. [PubMed: 21273505]
24. Ferreiro DU, Hegler JA, Komives EA, Wolynes PG. Localizing frustration in native proteins and protein assemblies. Proc Natl Acad Sci U S A. 2007; 104:19819–19824. [PubMed: 18077414]
25. Li W, Wolynes PG, Takada S. Frustration, specific sequence dependence, and nonlinearity in large-amplitude fluctuations of allosteric proteins. Proc Natl Acad Sci U S A. 2011; 108:3504–3509. [PubMed: 21307307]
26. Yonemoto W, Garrod SM, Bell SM, Taylor SS. Identification of phosphorylation sites in the recombinant catalytic subunit of cAMP-dependent protein kinase. J Biol Chem. 1993; 268:18626–18632. [PubMed: 8395513]
27. Joseph RE, et al. Activation loop dynamics determine the different catalytic efficiencies of B cell- and T cell-specific tec kinases. Sci Signal. 2013; 6(290):ra76. [PubMed: 23982207]
28. Xie Q, Joseph RE, Fulton DB, Andreotti AH. Substrate recognition of PLCgamma1 via a specific docking surface on Itk. J Mol Biol. 2013; 425:683–696. [PubMed: 23219468]
29. Zhu G, Xia Y, Nicholson LK, Sze KH. Protein dynamics measurements by TROSY-based NMR experiments. J Magn Reson. 2000; 143:423–426. [PubMed: 10729271]
30. Palmer AG 3rd, Kroenke CD, Loria JP. Nuclear magnetic resonance methods for quantifying microsecond-to-millisecond motions in biological macromolecules. Methods Enzymol. 2001; 339:204–238. [PubMed: 11462813]
31. Chen J, Stites WE. Packing is a key selection factor in the evolution of protein hydrophobic cores. Biochemistry. 2001; 40:15280–15289. [PubMed: 11735410]
32. Tyrrell C, et al. Isoleucine/leucine2 is essential for chemoattractant activity of beta-defensin Defb14 through chemokine receptor 6. Mol Immunol. 2010; 47:1378–1382. [PubMed: 20022113]
33. Cornish VW, Kaplan MI, Veenstra DL, Kollman PA, Schultz PG. Stabilizing and destabilizing effects of placing beta-branched amino acids in protein alpha-helices. Biochemistry. 1994; 33:12022–12031. [PubMed: 7918421]
34. Gallagher SJ, et al. p16INK4a expression and absence of activated B-RAF are independent predictors of chemosensitivity in melanoma tumors. Neoplasia. 2008; 10:1231–1239. [PubMed: 18953432]
35. Muzny, et al. Comprehensive molecular characterization of human colon and rectal cancer. Nature. 2012; 487:330–337. [PubMed: 22810696]
36. Vipond IB, Moon BJ, Halford SE. An isoleucine to leucine mutation that switches the cofactor requirement of the EcoRV restriction endonuclease from magnesium to manganese. Biochemistry. 1996; 35:1712–1721. [PubMed: 8639650]
37. Herrera D, et al. A single residue in the S6 transmembrane domain governs the differential flecainide sensitivity of voltage-gated potassium channels. Mol Pharmacol. 2005; 68:305–316. [PubMed: 15883204]
38. Vestergaard AL, et al. Critical roles of isoleucine-364 and adjacent residues in a hydrophobic gate control of phospholipid transport by the mammalian P4-ATPase ATP8A2. Proc Natl Acad Sci U S A. 2014; 111:E1334–1343. [PubMed: 24706822]

39. Dagil R, et al. The WSXWS motif in cytokine receptors is a molecular switch involved in receptor activation: insight from structures of the prolactin receptor. Structure. 2012; 20:270–282. [PubMed: 22325776]
40. Meharena HS, et al. Deciphering the structural basis of eukaryotic protein kinase regulation. PLoS Biol. 2013; 11(10):e1001680. [PubMed: 24143133]
41. Eisenmesser EZ, Bosco DA, Akke M, Kern D. Enzyme dynamics during catalysis. Science. 2002; 295:1520–1523. [PubMed: 11859194]
42. Henzler-Wildman KA, et al. A hierarchy of timescales in protein dynamics is linked to enzyme catalysis. Nature. 2007; 450:913–916. [PubMed: 18026087]
43. Henzler-Wildman KA, et al. Intrinsic motions along an enzymatic reaction trajectory. Nature. 2007; 450:838–844. [PubMed: 18026086]
44. Shan Y, Arkhipov A, Kim ET, Pan AC, Shaw DE. Transitions to catalytically inactive conformations in EGFR kinase. Proc Natl Acad Sci U S A. 2013; 110:7270–7275. [PubMed: 23576739]
45. Sali A, Blundell TL. Comparative protein modelling by satisfaction of spatial restraints. J Mol Biol. 1993; 234:779–815. [PubMed: 8254673]
46. Krivov GG, Shapovalov MV, Dunbrack RL Jr. Improved prediction of protein side-chain conformations with SCWRL4. Proteins. 2009; 77:778–795. [PubMed: 19603484]
47. MacKerell AD Jr, Banavali N, Foloppe N. Development and current status of the CHARMM force field for nucleic acids. Biopolymers. 2000; 56:257–265. [PubMed: 11754339]
48. Phillips JC, et al. Scalable molecular dynamics with NAMD. J Comput Chem. 2005; 26:1781–1802. [PubMed: 16222654]
49. Humphrey W, Dalke A, Schulten K. VMD: visual molecular dynamics. J Mol Graph. 1996; 14:33–38. 27–38. [PubMed: 8744570]
50. Jenik M, et al. Protein frustratometer: a tool to localize energetic frustration in protein molecules. Nucleic Acids Res. 2012; 40(Web Server issue):W348–351. [PubMed: 22645321]
51. DeLano, WL. The PyMOL Molecular Graphics System. DeLano Scientific; San Carlos, CA, USA: 2002.
52. Joseph RE, Xie Q, Andreotti AH. Identification of an allosteric signaling network within Tec family kinases. J Mol Biol. 2010; 403:231–242. [PubMed: 20826165]
53. Seeliger MA, et al. High yield bacterial expression of active c-Abl and c-Src tyrosine kinases. Protein Sci. 2005; 14:3135–3139. [PubMed: 16260764]
54. Johnson BA, Blevins RA. NMRView: A computer program for the visualization and analysis of NMR data. J Biomol NMR. 1994; 4:603–614. [PubMed: 22911360]
55. Wales TE, Fadgen KE, Gerhardt GC, Engen JR. High-speed and high-resolution UPLC separation at zero degrees Celsius. Anal Chem. 2008; 80:6815–6820. [PubMed: 18672890]
56. Choi SH, et al. Conformational locking upon cooperative assembly of notch transcription complexes. Structure. 2012; 20:340–349. [PubMed: 22325781]
57. Wales TE, Engen JR. Hydrogen exchange mass spectrometry for the analysis of protein dynamics. Mass Spectrom Rev. 2006; 25:158–170. [PubMed: 16208684]
58. Zhang Z, Smith DL. Determination of amide hydrogen exchange by mass spectrometry: a new tool for protein structure elucidation. Protein Sci. 1993; 2:522–531. [PubMed: 8390883]
59. Houde D, Berkowitz SA, Engen JR. The utility of hydrogen/deuterium exchange mass spectrometry in biopharmaceutical comparability studies. J Pharm Sci. 2011; 100:2071–2086. [PubMed: 21491437]
60. Scouras AD, Daggett V. The Dynameomics rotamer library: amino acid side chain conformations and dynamics from comprehensive molecular dynamics simulations in water. Protein Sci. 2011; 20:341–352. [PubMed: 21280126]

Highlights

- Tec family kinases mediate the immune response and contain catalytic domains that are inactive by default.
- Molecular dynamics simulations identify an isoleucine in the N-lobe that maintains the inactive state of the Btk kinase.
- Conservative mutation of isoleucine to leucine abolishes the ‘inactive by default’ status of the Btk kinase domain.
- Unique conformational requirements of the beta-branched isoleucine side chain create a wedge that sterically prevents sampling of the active state; mutation to a leucine side chain removes the steric impediment, allowing increased population of the active conformation.

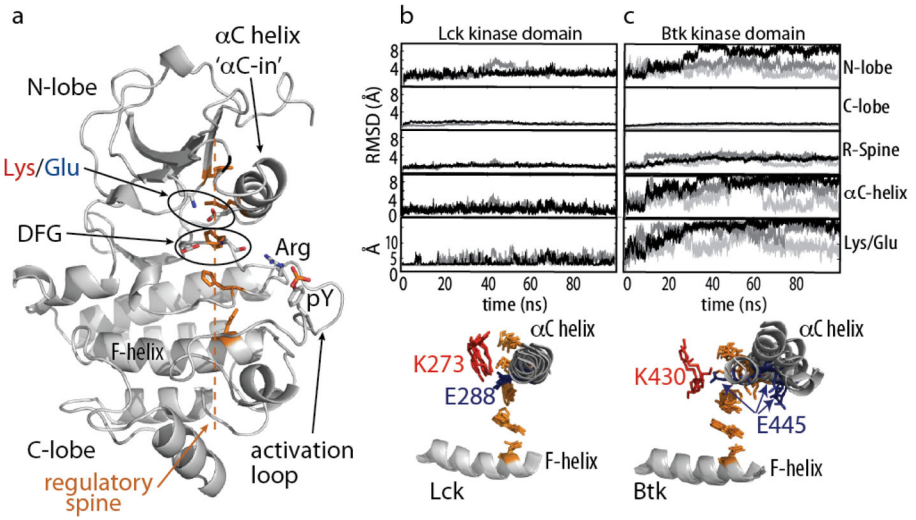

Figure 1. Molecular dynamics simulations reveal differences between the Btk and Lck kinase domains

(a) Structure of a kinase domain in the active conformation. Key structural motifs that stabilize the active state are indicated. The regulatory spine residues are orange and indicated with the dotted line, the DFG motif and conserved Lys/Glu salt bridge are circled, the αC helix is in the αC-in conformation, and the activation loop tyrosine is phosphorylated (pY) and contacting the conserved arginine. (b) 100 nanosecond (ns) equilibrium simulations were performed for (b) active Lck (PDB ID: 3LCK; residues 239–501) and (c) active Btk (PDB ID: 3K54; residues 396–659). Root mean square deviation (RMSD) from the starting structure is reported for select regions of each kinase domain: the amino-terminal lobe (N-lobe), the carboxy-terminal lobe (C-lobe), the regulatory spine (R-spine), and the αC helix. The distance (Å) between the lysine/glutamate side chains (K273/E288 for Lck and K430/E445 for Btk) are shown over the course of the simulations. Replica 1 is shown in black, 2 in dark gray, and 3 in light gray. Snapshots of the catalytic core during the simulations from replica 1 of Lck and replica 1 of Btk are shown at 0ns, 10ns, 20ns, 30ns, 40ns, 50ns, and 100ns. For each structural superposition the lysine and glutamate side chains are red and blue, respectively, the regulatory spine residues are orange and the αC helix and F helix are labeled.

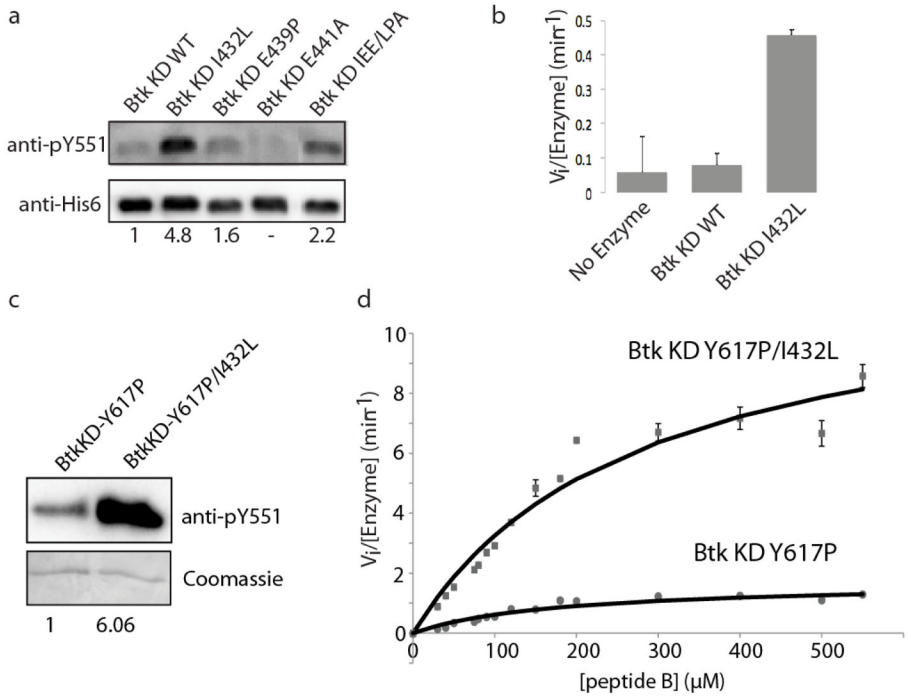

Figure 2. Mutation of I432 to leucine relieves the 'inactive by default' status of the Btk kinase domain

(a) *In vitro* kinase assays for His6-tagged Btk kinase domain variants: wild type (WT) Btk kinase domain, three single Btk kinase domain mutants: Btk I432L, Btk E439P, and Btk E441A, and the Btk kinase domain triple mutant: Btk IEE/LPA (I432L/E439P/E441A). Btk activity is monitored by autophosphorylation using the anti-phosphotyrosine antibody, anti-pY551, that is specific for phosphorylation on the activation loop (pY551) of Btk. Tyrosine phosphorylation levels were quantified and normalized to total protein in each lane (pY551 for wild type Btk kinase is set to 1). In (a)–(d), KD refers to the isolated Btk kinase domain. (b) Initial velocity measurements for wild type Btk kinase domain (Btk WT) and the Btk I432L kinase domain mutant (Btk I432L) using the poly (4:1 Glu, Tyr) peptide substrate. (c) Same experiment as shown in panel (a) comparing autophosphorylation of Btk kinase domain Y617P and Btk kinase domain Y617P/I432L following overnight incubation with ATP. Coomassie staining is used to show enzyme levels. (d) Peptide substrate curves for Btk kinase domain Y617P (circles) and Btk kinase domain Y617P/I432L (squares), were fit to the Michaelis-Menten equation using GraphFit to obtain kinetic parameters.

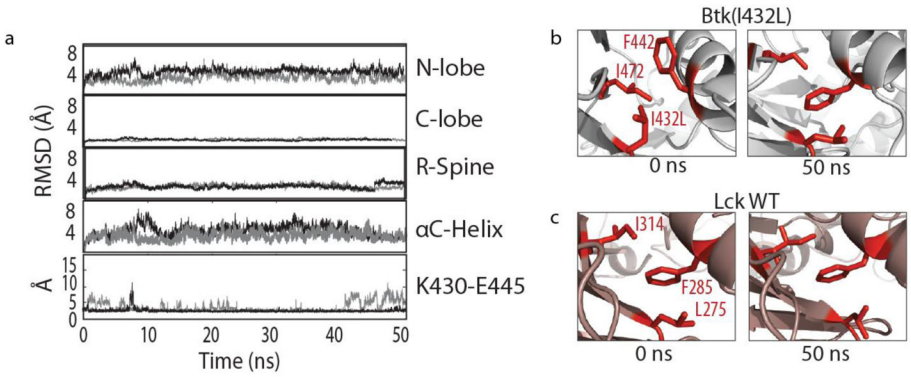

Figure 3. Btk I432L behaves like Lck kinase domain in MD simulations

(a) 50 nanosecond (ns) equilibrium simulations were performed for Btk I432L. Root mean square deviation (RMSD) from the starting structure is reported for select regions of the kinase domain as in Figure 1b and c. Replica 1 is shown in black, replica 2 in dark gray. (b,c) Snapshots of the 0 and 50 ns time-points from the simulation of Btk I432L (b) and wild type Lck (c). The side chains for the phenylalanine on the αC helix (F442 for Btk, F285 for Lck) and adjacent to the αC helix (I314 (Lck), L275 (Lck) and I472 (Btk)) are shown in red and labeled. The site of mutation in Btk is labeled as I432L and the side chain in the structure is the non-native leucine. The chi1 dihedral angle is defined by N-Cα-Cβ-Cγ for leucine (N-Cα-Cβ-Cγ1 for isoleucine).

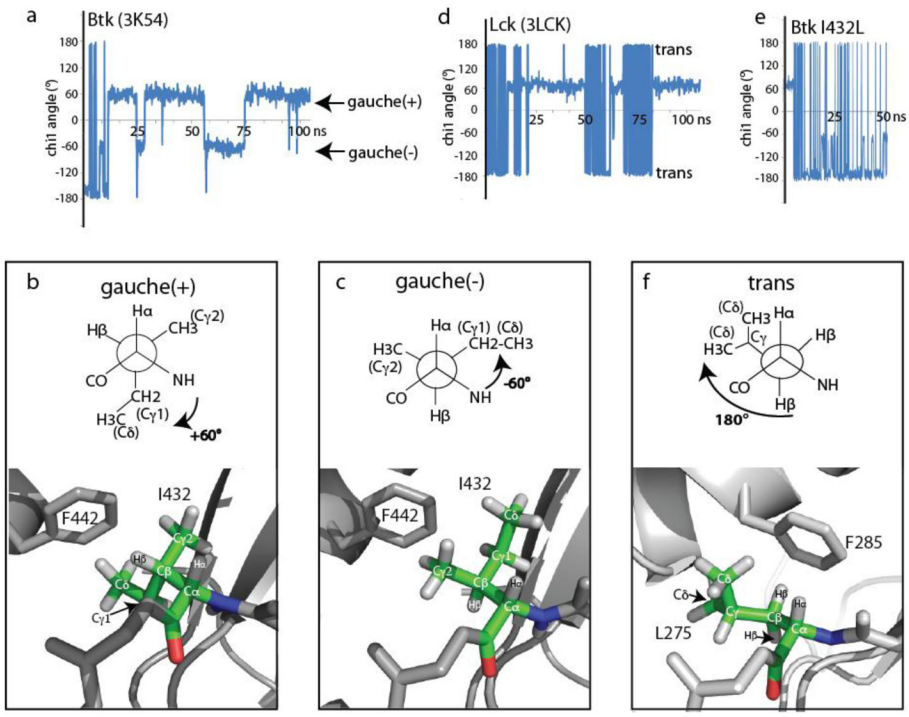

Figure 4. Isoleucine and leucine side chain rotamer preferences differ between wild type Btk and the Btk I432L mutant

(a) I432 chi1 angles are shown during the Btk kinase domain simulation. Gauche(+) and gauche(−) are indicated at +60° and −60°, respectively. The preference for gauche(+) and gauche(−) in the Btk simulations is consistent with the probabilities of isoleucine rotamers observed in analyses of rotamer libraries (60). (b,c) Newman projections for each isoleucine chi1 rotamer are shown above snapshots from the simulations showing I432 in the gauche(+) rotamer conformation (b) and the gauche(−) rotamer conformation (c). (d,e) Chi1 angles for (d) L275 of Lck and (e) L432 of the Btk I432L mutant shown over the course of the simulation. Chi1 angles shown are from a single replicate and are representative of all simulations for each protein. (f) Newman projection for the trans leucine chi1 rotamer is shown above the crystal structure of the Lck kinase domain (3LCK) showing the trans rotamer for L275.

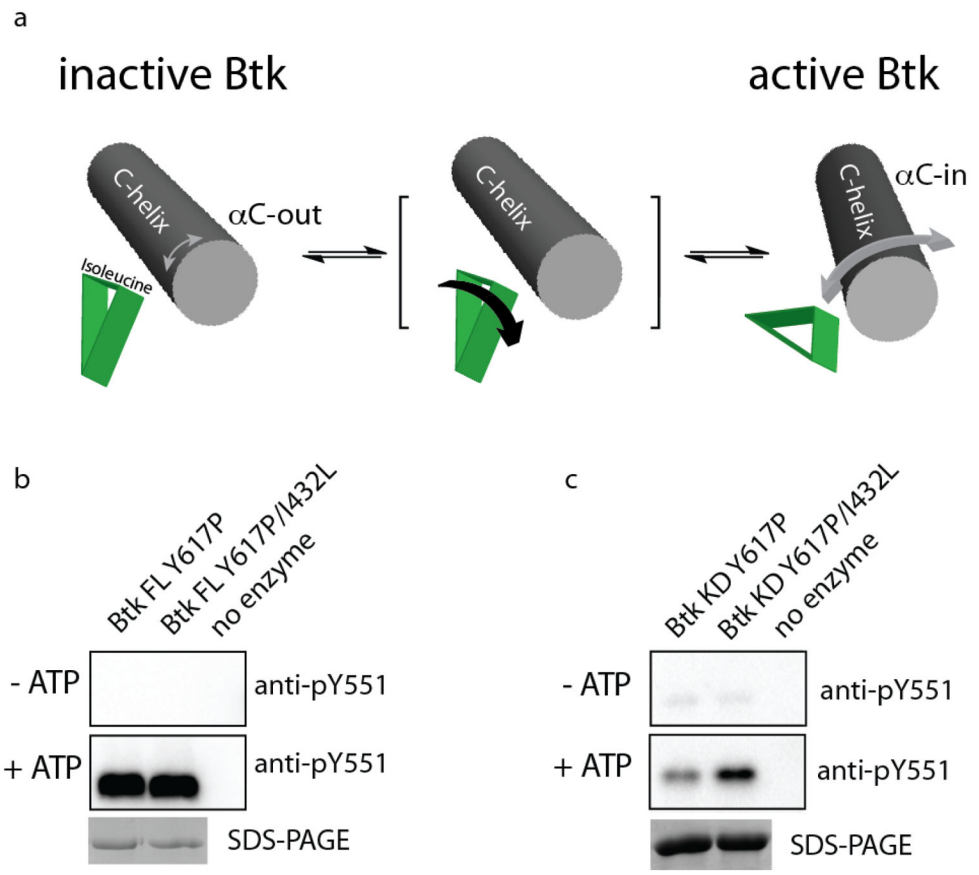

Figure 5. Isoleucine 432 in the Btk kinase domain sterically blocks the αC-in conformation associated with the active kinase domain

(a) Model describing the proposed steric wedge created by specific rotamer conformations of I432 in the isolated Btk kinase domain. In inactive Btk, the αC helix samples a smaller range of conformations that favor αC-out (small grey doubled headed arrow). The intermediate state indicates that the putative steric block created by I432 can be relieved either by mutation to leucine (favoring the trans rotamer) or by a shift to the isoleucine trans chi1 rotamer (indicated by black arrow). The rotamer shift for the I432 side chain may be energetically favored by association of the Btk regulatory domains with the N-lobe of the kinase domain. In the active state, the αC helix samples greater conformational space including the αC-in conformation (large grey doubled headed arrow). (b & c) Comparison of (b) full length Btk (Btk FL Y617P) and full length Btk containing the I432L mutation (Btk FL Y617P/I432L) and (c) isolated Btk kinase domain (Btk KD Y617P) and isolated Btk kinase domain containing the I432L mutation (Btk KD Y617P/I432L). In both experiments the top panel shows activation loop phosphorylation levels (pY551) prior to incubation with ATP and the middle panel shows pY551 levels after incubation with ATP. Bottom panel shows enzyme levels.

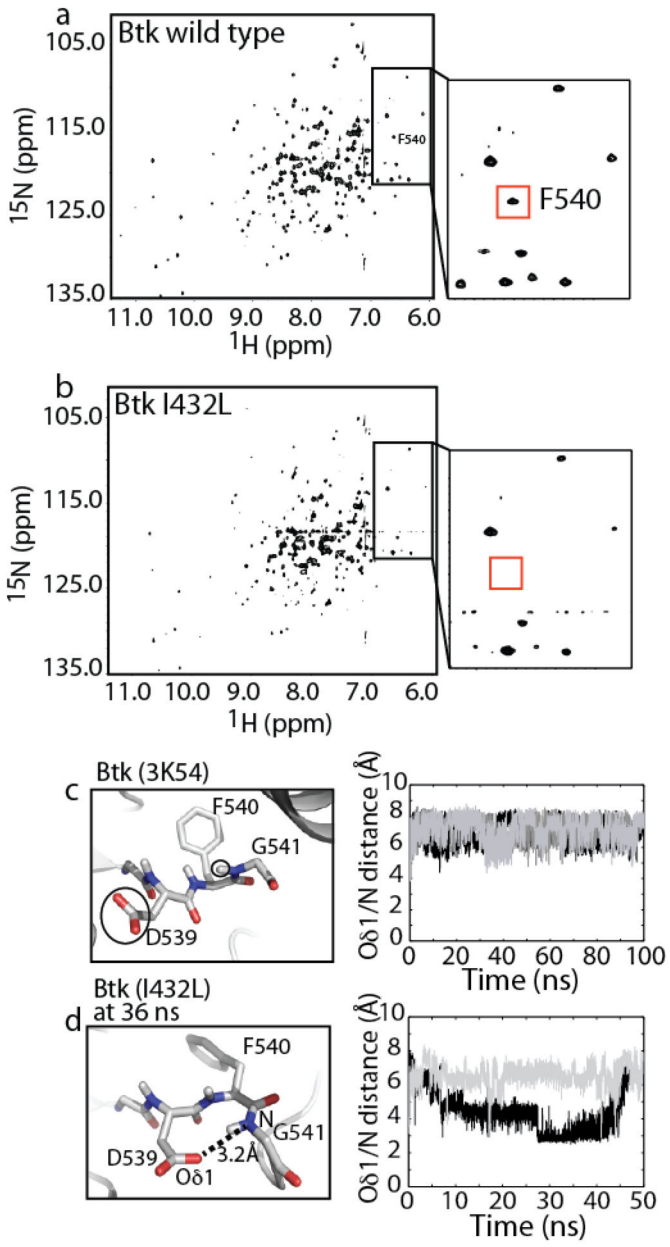

Figure 6. NMR spectroscopy and simulation data suggest differences in the DFG motif between wild type Btk and the Btk I432L mutant

(a) ^{1}H-^{15}N TROSY HSQC spectrum of uniformly ^{15}N labeled Btk kinase domain. The amide resonance for F540 is labeled in the complete spectrum and labeled in the region of the spectrum shown in the insert. (b) ^{1}H-^{15}N TROSY HSQC spectrum of uniformly ^{15}N labeled Btk I432L kinase domain. In this spectrum, the resonance for F540 is not detected (red box indicates expected position of the F540 amide peak; no new peaks appear suggesting line broadening rather than a change in chemical shift). (c) *Left,* Structure of the DFG motif in the Btk crystal structure. The side chains of D539, F540 and G541 are labeled and the carboxylate of the D539 side chain and the NH group of G541 are circled. *Right,* The distance (Å) between the carboxylate oxygen (Oδ1) of D539 and the amide nitrogen (N)

of G541 is plotted for the three replicates of the 100 ns Btk simulations. (d) *Left,* Structural snapshot from the Btk I432L simulation showing the conformation of the DFG motif at 36 ns. The short distance (3.2 Å) between D539 Oδ1 and G541 N is shown with a dotted line. *Right,* Same as described for (c) showing the D539 Oδ1 - G541 N distance for two replicates of the 50 ns Btk I432L simulations.

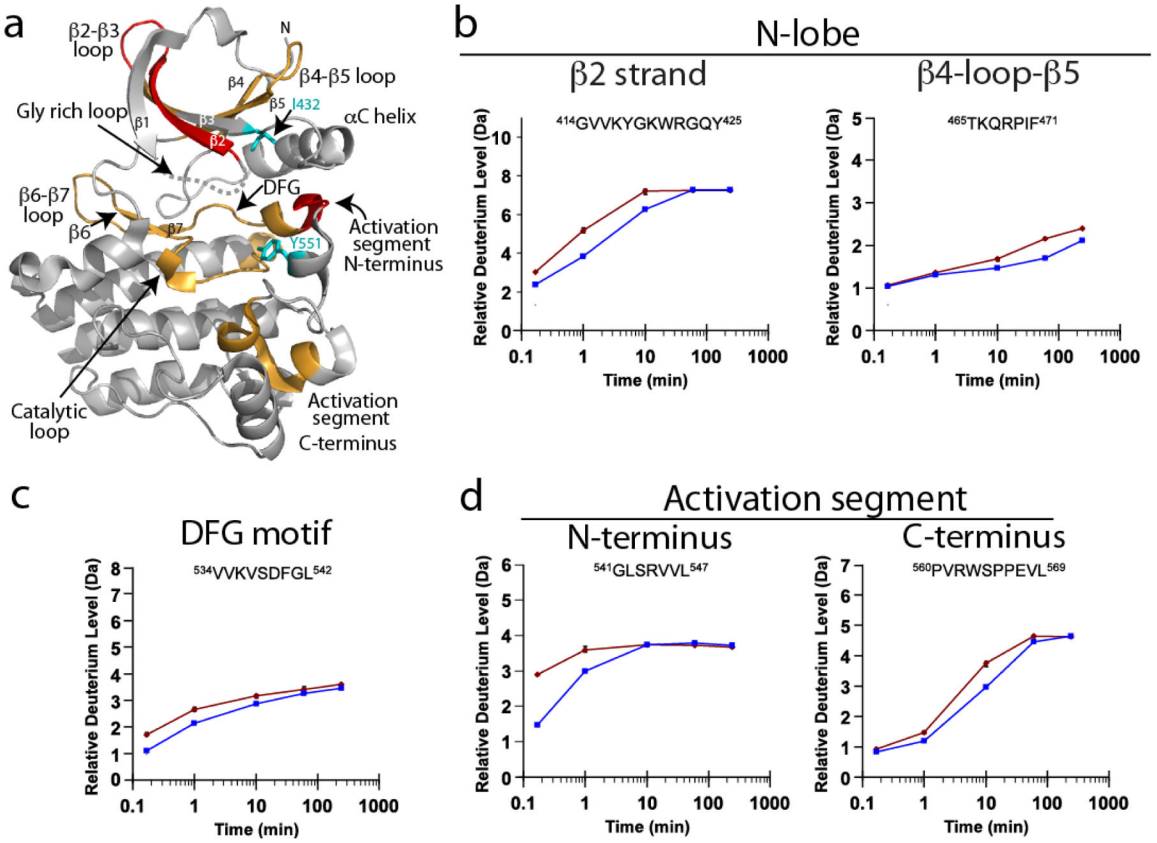

Figure 7. Hydrogen/deuterium exchange mass spectrometry (HDXMS) indicates increased conformational flexibility in the active Btk I432L mutant

(a) HDXMS results are illustrated on the structure of the Btk kinase domain. The Btk structure used here is the inactive conformation (3GEN) since the activation loop is visible in this structure. Increased deuterium uptake is seen in the Btk I432L mutant for regions shown in red (greater than 0.8 Da increase in mass), and orange (0.5 to 0.8 Da increase in mass). The side chains of I432 and Y551 (phosphorylation site on the activation loop) are labeled and colored cyan. (b–d) Deuterium exchange was measured for the WT Btk kinase domain (blue squares) and Btk I432L (red circles) and data were plotted as relative deuterium incorporation versus time for peptides covering specific regions of secondary structure within the N-lobe (b), DFG motif (c), and the N-terminus and C-terminus of the Btk activation segment (d). The data are an average of two independent labeling replicates. Error bars shown indicate the absolute range of relative deuterium level and in most cases are within the size of the data point.